

PCCP

Accepted Manuscript



This is an *Accepted Manuscript*, which has been through the Royal Society of Chemistry peer review process and has been accepted for publication.

Accepted Manuscripts are published online shortly after acceptance, before technical editing, formatting and proof reading. Using this free service, authors can make their results available to the community, in citable form, before we publish the edited article. We will replace this *Accepted Manuscript* with the edited and formatted *Advance Article* as soon as it is available.

You can find more information about *Accepted Manuscripts* in the [Information for Authors](#).

Please note that technical editing may introduce minor changes to the text and/or graphics, which may alter content. The journal's standard [Terms & Conditions](#) and the [Ethical guidelines](#) still apply. In no event shall the Royal Society of Chemistry be held responsible for any errors or omissions in this *Accepted Manuscript* or any consequences arising from the use of any information it contains.

Quantum interference and electron correlation in charge transport through triangular quantum dot molecules[†]

Chih-Chieh Chen,^a Yia-chung Chang,^{*abc} and David M T Kuo^{*d}

Received Xth XXXXXXXXXXXX 20XX, Accepted Xth XXXXXXXXXXXX 20XX

First published on the web Xth XXXXXXXXXXXX 200X

DOI: 10.1039/b000000x

We study the charge transport properties of triangular quantum dot molecule (TQDM) connected to metallic electrodes, taking into account all correlation functions and relevant charging states. The quantum interference (QI) effect of TQDM resulting from electron coherent tunneling between quantum dots is revealed and well interpreted by the long distance coherent tunneling mechanism. The spectra of electrical conductance of TQDM with charge filling from one to six electrons clearly depict the many-body and topological effects. The calculated charge stability diagram for conductance and total occupation numbers match well with the recent experimental measurements. We also demonstrate that the destructive QI effect on the tunneling current of TQDM is robust with respect to temperature variation, making the single electron QI transistor feasible at higher temperatures.

1 Introduction

Molecule transistors (MTs) provide a brightened scenario of nanoelectronics with low power consumption.^{1–3} To date, the implementation of MTs remains challenging, and a good theoretical understanding of their characteristics is essential for advancing the technology. The current-voltage (I-V) curves of MTs are typically predicted by calculations based on the density functional theory (DFT).³ However, the DFT approach cannot fully capture the correlation effect in the transport behavior of MTs in the Coulomb-blockade regime. A theoretical framework to treat adequately the many-body problem of a molecular junction remains elusive due to the complicated quantum nature of such devices. Experimental studies of a artificial molecule with simplified structures are important not only for the advances of novel nanoelectronics, but also for providing a testing ground of many body theory. For example, the coherent tunneling between serially coupled double quantum dots (DQDs) was studied and demonstrated for application as a spin filter in the Pauli spin blockade regime.⁴ Recent experimen-

tal studies have been extended to serially coupled triple quantum dots (SCTQDs) for studying the effect of long distance coherent tunneling (LDCT) in electron transport.^{5–7} Triangular quantum dot molecule (TQDM) provides the simplest topological structure with quantum interference (QI) phenomena.^{8–10} The QI effect in the coherent tunneling process of TQDM junctions has been studied experimentally.^{11,12}

It was suggested that the tunneling currents through benzene molecules can also show a destructive QI behavior.^{3,9} The tunneling current through a single benzene molecule was theoretically studied by DFT.⁹ However, the influence of the strong correlation on the QI effect remains unclear due to the limitation of DFT. Many theoretical works have pointed out that electron Coulomb interactions have strong influence not only on the electronic structures of TQDM,^{13,14} but also on the probability weights of electron transport paths.^{15–18} When both the intradot and interdot Coulomb interactions in a TQDM are included, the transport behavior involving multiple electrons becomes quite complicate. The setup for the TQDM junction of interest is depicted in Fig. 1. Here we present a full many-body solution to the tunneling current of TQDM, which can well illustrate the Pauli spin blockade effect of DQDs,⁴ LDCT of SCTQDs^{5–7} and QI of TQDMs¹¹ for both equilibrium and nonequilibrium cases. Thus, our theoretical work can provide useful guidelines for the design of future molecular electronics and the realization of large scale quantum registers built by multiple QDs.¹⁹

We adopt the equation of motion method (EOM),

[†] Electronic Supplementary Information (ESI) available. See DOI: 10.1039/b000000x/

^a Department of Physics, University of Illinois at Urbana-Champaign, Urbana, Illinois 61801, USA.

^b Research Center for Applied Sciences, Academia Sinica, Taipei, 11529 Taiwan. E-mail: yiachang@gate.sinica.edu.tw

^c Department of Physics, National Cheng-Kung University, Tainan, 70101 Taiwan.

^d Department of Electrical Engineering and Department of Physics, National Central University, Chungli, 320 Taiwan. E-mail: mtkuo@ee.ncu.edu.tw

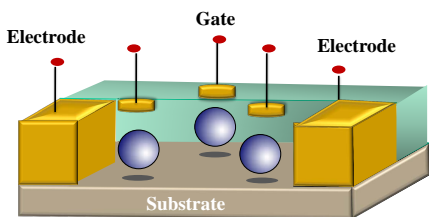


Fig. 1 Illustration of the TQDM junction system of interest.

which is a powerful tool for studying electron transport, taking into account electron Coulomb interactions.^{15–18} This method has been applied to reveal the transport behaviors of a single QD with multiple energy levels¹⁶ and DQDs.^{17,18} For a TQDM with one level per QD, there are 64 configurations for electrons to transport between electrodes.²⁰ Previous theoretical works have ignored the high-order Green functions resulting from electron Coulomb interactions to simplify the calculation.²⁰ To have a full solution becomes crucial for depicting the charge transport involving a few electrons. We solve the EOM of Green functions up to six electrons, taking into account all correlations caused by electron Coulomb interactions and electron hopping between TQDM. This involves solving 4752 Green's functions and 923 correlation functions self-consistently.

2 Model

We consider an artificial molecule made of nanoscale QDs, in which the energy level separations are much larger than the on-site Coulomb interactions and thermal energies. Thus, only one energy level for each quantum dot is included. The extended Hubbard-Anderson model is employed to simulate the TQDM junction with Hamiltonian given by $H = H_0 + H_T + H_{QDs}$, where $H_0 = \sum_{\mathbf{k},\sigma,\alpha} \epsilon_{\mathbf{k}} c_{\mathbf{k},\sigma,\alpha}^\dagger c_{\mathbf{k},\sigma,\alpha}$ is the Hamiltonian for free electrons in the electrodes. $c_{\mathbf{k},\sigma,\alpha}^\dagger (c_{\mathbf{k},\sigma,\alpha})$ creates (destroys) an electron of momentum \mathbf{k} and spin σ with energy $\epsilon_{\mathbf{k}}$ in the α electrode. $H_T = \sum_{\mathbf{k},\ell,\alpha} (V_{\mathbf{k},\alpha,\ell} c_{\mathbf{k},\sigma,\alpha}^\dagger d_{\ell,\sigma} + V_{\mathbf{k},\alpha,\ell}^* d_{\ell,\sigma}^\dagger c_{\mathbf{k},\sigma,\alpha})$. $V_{\mathbf{k},\alpha,\ell}$ describes the coupling between the α electrode and the ℓ -th QD. $d_{\ell,\sigma}^\dagger (d_{\ell,\sigma})$ creates (destroys) an electron in the ℓ -th dot. H_{QDs} is the extended

Hubbard Hamiltonian for multiple QDs.

$$H_{QDs} = \sum_{\ell,\sigma} E_\ell n_{\ell,\sigma} + \sum_{\ell} U_\ell n_{\ell,\sigma} n_{\ell,\bar{\sigma}} + \sum_{\ell < j, \sigma, \sigma'} U_{\ell j} n_{\ell,\sigma} n_{j,\sigma'} + \sum_{\ell \neq j, \sigma} t_{\ell j} d_{\ell,\sigma}^\dagger d_{j,\sigma}, \quad (1)$$

where E_ℓ is the spin-independent QD energy level, $n_{\ell,\sigma} = d_{\ell,\sigma}^\dagger d_{\ell,\sigma}$, U_ℓ and $U_{\ell j}$ ($\ell < j$) denote the intradot and interdot Coulomb interactions, respectively and $t_{\ell j}$ describes the electron interdot coupling. The interdot Coulomb interactions as well as intradot Coulomb interactions are important for nanoscale semiconductor QDs and molecules. Therefore, $U_{\ell,j}$ cannot be ignored.

Using the Keldysh-Green's function technique^{15,21}, the electrical current from reservoir α to the TQDM junction is calculated according to the Meir-Wingreen formula

$$J_\alpha = \frac{ie}{h} \int d\epsilon \sum_{j\sigma} \Gamma_j^\alpha [G_{j\sigma}^<(\epsilon) + f_\alpha(\epsilon)(G_{j\sigma}^r(\epsilon) - G_{j\sigma}^a(\epsilon))], \quad (2)$$

where $\Gamma_j^\alpha(\epsilon) = \sum_{\mathbf{k}} |V_{\mathbf{k},\alpha,j}|^2 \delta(\epsilon - \epsilon_{\mathbf{k}})$ is the tunneling rate between the α -th reservoir and the j -th QD. Throughout the paper, for two-terminal devices we assume that the left (right) lead is only coupled to the left (right) QD with tunneling rate Γ_L (Γ_R), while there is no coupling between the center QD and the two leads. For three-terminal devices, the coupling between the center QD and a third gate is described by the tunneling rate Γ_C . $f_\alpha(\epsilon) = 1/\{\exp[(\epsilon - \mu_\alpha)/k_B T] + 1\}$ denotes the Fermi distribution function for the α -th electrode, where μ_α is the chemical potential and T is the temperature of the system. e , h , and k_B denote the electron charge, the Planck's constant, and the Boltzmann constant, respectively. $G_{j\sigma}^<(\epsilon)$, $G_{j\sigma}^r(\epsilon)$, and $G_{j\sigma}^a(\epsilon)$ are the frequency domain representations of the one-particle lesser, retarded, and advanced Green's functions $G_{j\sigma}^<(t, t') = i\langle d_{j,\sigma}^\dagger(t') d_{j,\sigma}(t) \rangle$, $G_{j\sigma}^r(t, t') = -i\theta(t - t')\langle \{d_{j,\sigma}(t), d_{j,\sigma}^\dagger(t')\} \rangle$, and $G_{j\sigma}^a(t, t') = i\theta(t' - t)\langle \{d_{j,\sigma}(t), d_{j,\sigma}^\dagger(t')\} \rangle$, respectively. These one-particle Green's functions are related recursively to other Green's functions and correlators via the many-body equation of motion,^{16–18} which we solve via an iterative numerical procedure to obtain all n -particle Green's functions ($n = 1, \dots, 6$) and correlators for the TQDM. (See supplemental materials.) Our procedure is valid in the Coulomb blockade regime, but not the Kondo regime.^{22,23} Throughout this paper, we assume the on-site Coulomb interaction $U_\ell = U_0 = 100\Gamma_0$ for all three QDs and the same tunneling rates at all leads, $\Gamma_j^\alpha = \Gamma$ with j labeling the QD directly connected to lead α .

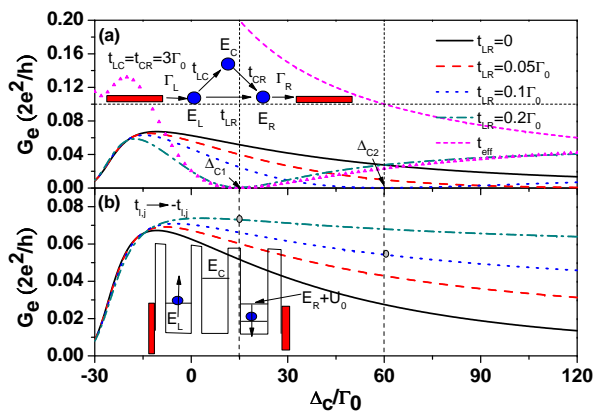


Fig. 2 Electrical conductance (G_e) of TQDM as a function of central QD energy for different t_{LR} strengths in the Pauli spin blockade configuration with $E_L = E_F$ and $E_R = E_F - U_R$. (a) $t_{LC} = t_{CR} = 3\Gamma_0$, and (b) $t_{\ell,j}$ replaced by $-t_{\ell,j}$. Other physical parameters are $k_B T = 1\Gamma_0$, $\Gamma = 0.3\Gamma_0$, $U_{LC} = U_{CR} = 30\Gamma_0$, and $U_{LR} = 0$.

3 Results and discussion

Although the QI of TQDM was theoretically investigated previously^{24,25}, the effect of intradot and interdot Coulomb interactions was not considered. Here, we utilize the LDCT effect to tune the effective hopping strength between outer QDs to achieve the destructive and constructive QIs in the presence of electron Coulomb interaction. We consider a TQDM junction in the Pauli spin blockade (PSB) configuration^{4,18} with $E_L = E_F$, $E_R = E_F - U_0$, $t_{LC} = t_{CR} = 3\Gamma_0$, $\Gamma_L = \Gamma_R = 0.3\Gamma_0$, $U_{LC} = U_{CR} = 30\Gamma_0$, and $U_{LR} = 0$. Fig. 2(a) shows the electrical conductance (G_e) as a function of central QD energy level ($\Delta_C = E_C - E_F$) for t_{LR} varying from 0 to $0.2\Gamma_0$ at $k_B T = 1\Gamma_0$ (in weak interdot coupling regime). For Δ_C less than $-15\Gamma_0$, G_e is not sensitive to the variation of t_{LR} , indicating that the transport is mainly through the upper path involving the center QD as shown in the inset of Fig. 2(a). In the case of $t_{LR} = 0$, G_e can be well explained by the LDCT effect when E_C is far away from E_F .²⁶ The central QD provides an intermediated state for electrons in the outer QDs. Through the upper path, TQDM behaves like a double QD with an effective hopping $t_{eff} = -t_{LC}t_{CR}/(U_{CR} + \Delta_C)$, which can also be understood by the second order perturbation theory.²⁶ Once $t_{LR} \neq 0$ (the lower path turns on), electron transport through the two paths with t_{eff} and t_{LR} lead to a destructive QI. Note that G_e for the case of $t_{LR} \neq 0$ is reduced compared to the case of $t_{LR} = 0$. In particular,

G_e is vanishingly small at the value of Δ_C where $|t_{eff}|$ crosses t_{LR} as indicated by dashed lines in Fig. 2(a). For illustration, the curve for $|t_{eff}| = |t_{LC}t_{CR}|/(U_{CR} + \Delta_C)$ is also shown in Fig. 2(a). (See short-dashed curve) The vanishing G_e occurs at lower Δ_C with increasing $|t_{LR}|$ (Compare dash-dotted with dashed curves). Due to topological effect, the electron-hole symmetry does not hold for the energy spectrum of TQDM.¹³ When TQDM has identical QD energy levels ($E_\ell = E_0$) and homogeneous electron hopping strengths $t_{\ell,j} = t$, we have one level $\epsilon = E_0 + 2t$ and one doubly degenerate level with $\epsilon = E_0 - t$ for the case of $U_\ell = U_{\ell,j} = 0$. Unlike the cases of DQDs and SCTQDs, the lowest energy level depends on the sign of $t_{\ell,j}$. This is a manifesting result of electron-hole asymmetrical behavior of TQDM. Therefore, it will be interesting to examine the sign effect of $t_{\ell,j}$ on the QI behavior. Physically, the sign of $t_{\ell,j}$ depends on the symmetry properties of orbitals, which can change in different configurations. We can replace $t_{\ell,j}$ by $-t_{\ell,j}$ to examine the QI effect with respect to the electron-hole symmetry. The results are shown in Fig. 2(b). We find that G_e is enhanced with increasing t_{LR} , which is attributed to the constructive QI effect, in contrast to the destructive QI effect shown in Fig. 2(a).

To gain deeper understanding of the destructive and constructive QI shown in Fig. 2, we compare our full calculation with the weak interdot-coupling theory,^{18,26} which allows simple closed-form expression for the electrical conductance of TQDM. We obtain $G_e = 2e^2/h \int d\epsilon \mathcal{T}(\epsilon) [\partial f(\epsilon)/\partial E_F] \approx (2e^2/h) \mathcal{T}(E_F)$ at low-temperature limit, where the transmission coefficient $\mathcal{T}(\epsilon)$ with 64 configurations is approximately given by

$$\mathcal{T}_{PSB}(\epsilon) = \frac{4\Gamma_L\Gamma_R P_{PSB} F_{QI}}{|\mu_1\mu_2\mu_3 - t_{CR}^2\mu_1 - t_{LC}^2\mu_3 - t_{LR}^2\mu_2 - 2t_{LR}t_{LC}t_{CR}|^2}, \quad (3)$$

where $F_{QI} = \mu_2^2(t_{LC}t_{CR}/\mu_2 + t_{LR})^2$ is a factor related to QI. $\mu_1 = \epsilon - E_L + i\Gamma_L$, $\mu_2 = \epsilon - E_C - U_{RC}$ and $\mu_3 = \epsilon - E_R - U_R + i\Gamma_R$. P_{PSB} denotes the probability weight in the PSB configuration.¹⁸ From Eq. (3), we have

$$G_e = \frac{2e^2}{h} \frac{P_{PSB} 4\Gamma^2 (t_{eff} + t_{LR})^2}{(\Gamma^2 + 2t_{eff}t_{LR} + t_{LR}^2)^2 + \Gamma^2 (t_{h1} + t_{h2})^2}, \quad (4)$$

where $t_{eff} = -t_{LC}t_{CR}/(U_{CR} + \Delta_C)$, $t_{h1} = -t_{LC}^2/(U_{CR} + \Delta_C)$, and $t_{h2} = -t_{CR}^2/(U_{CR} + \Delta_C)$ with $\Gamma_L = \Gamma_R \equiv \Gamma$. For $t_{LC} = t_{CR} = t_c = 0$, Eq. (4) reduces to the conductance of DQD,¹⁷ while for $t_{LR} = 0$, it reduces to the G_e of SCTQD.²⁶ At $\Delta_C = 15\Gamma_0$ and $60\Gamma_0$, which satisfy the condition of $t_{eff} + t_{LR} = 0$ for $t_{LR} = 0.2\Gamma_0$ and $t_{LR} = 0.1\Gamma_0$, respectively, and we see G_e vanishes

there. This well illustrates the destructive QI seen in Fig. 2(a). Once we make the substitution $t_{\ell,j} \rightarrow -t_{\ell,j}$ in Eq. (4), we can reveal the constructive QI in G_e as shown in Fig. 2(b). Note that in the weak coupling regime ($t_{eff}/\Gamma \ll 1$), the probability weight P_{PSB} of Eq. (4) calculated according to the procedures in Ref. 18, where the interdot two-particle correlation functions are factorized as the product of single occupation numbers, is consistent with the full calculation, but not for $t_{eff}/\Gamma \gg 1$. Away from the weak coupling regime, the interdot electron correlations become important. To explicitly reveal the importance of electron correlation effects, we plot the curve of $t_{LR} = 0.2\Gamma_0$ (with triangle marks) calculated by the procedure of Ref. 18 (including 64 configurations) in Fig. 2(a). Comparison between the full solution and the approximation considered in Ref. 18, we find that the electron correlation effects become very crucial when $t_{eff}/\Gamma \gg 1$. Once electron transport involves more electrons, the high-order (beyond two-particle) Green functions and correlation functions should be included (see the results of Fig. 3). The difference between the conventional mean-field theory of Ref. 3 with the full solution is even larger. The comparison between mean-field theory and the procedure of Ref. 18 has been discussed in the appendix of Ref. 18.

According to Eq. (4), constructive and destructive QI effects depend on the sign of $t_{\ell,j}$. Therefore, if the wavefunction of the center dot has opposite parity (say, an x -like state) with respect to the wavefunctions in two outer dots (assumed to be s -like), then t_{LC} will have opposite sign compared with t_{CR} and t_{LR} , and the sign of t_{eff} will be flipped. Consequently, the destructive QI shown in Fig. 2(a) will become constructive QI. Thus, for a center QD with an s -like ground state and an excited p -like state, it is possible to see the change of QI between destructive and constructive by tuning the gate voltage, which sweeps through different resonance energies of the center QD in addition to the change of sign of t_{eff} when the Fermi level goes from below the resonance level to above the resonance level. From the results of Fig. 2, QI effect can be electrically controlled by the energy level E_c . This advantage of TQDM may be useful for improving the spin filtering of DQDs⁴.

In addition to QI effects, spin frustration and topological effects (due to electron-hole asymmetry) on the measured quantities (electrical conductance or current) are also interesting issues.¹¹ Fig. 3(a) shows G_e as a function of gate voltage, Δ_g for $E_\ell = E_F + 10\Gamma_0 - \Delta_g$; $\ell = L, C, R$ at two different temperatures, $k_B T = 0$ and $1\Gamma_0$. Here, we consider the homogenous configuration with $U_{LR} = U_{LC} = U_{CR} = 30\Gamma_0$ and $t_{\ell,j} = t_c = 3\Gamma_0$. At low temperature, there are six main peaks in the G_e spec-

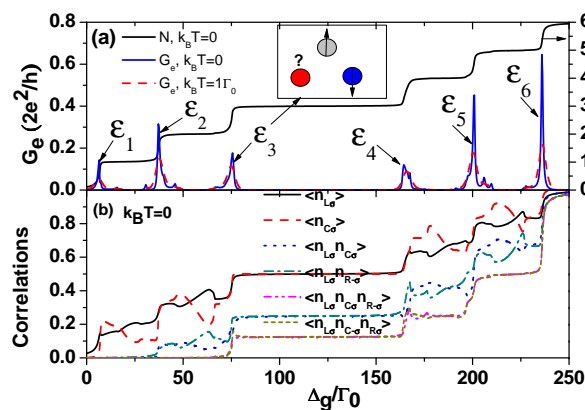


Fig. 3 (a) Electrical conductance of TQDMs as a function of gate voltage Δ_g with $E_L = E_R = E_C = E_F + 10\Gamma_0 - \Delta_g$ and $\Gamma = 1.6\Gamma_0$. (b) Correlation functions for $k_B T = 0\Gamma_0$. Other physical parameters are $t_{\ell,j} = 3\Gamma_0$ and $U_{LR} = U_{LC} = U_{CR} = 30\Gamma_0$.

trum, labeled by ϵ_n , $n = 1, \dots, 6$ and some secondary peaks. At higher temperature, the six main peaks are suppressed and broadened as shown by the dashed curve, and the secondary peaks are washed out. We also plot the total occupation number, $N = \sum_{\sigma} (N_{L,\sigma} + N_{R,\sigma} + N_{C,\sigma})$ as the black solid curve, which shows a stair-case behavior with plateaus at $N = 1, \dots, 6$, corresponding to the filling of TQDM with 1 to 6 electrons. It can be seen that the six main peaks occur at Δ_g where N is increased by 1. Thus, the peak positions ϵ_n correspond to the chemical potential of electrons in TQDM, i.e. the energy needed to add an electron to the system. The main peak positions can be approximately obtained by the calculation of chemical potential of TQDM without considering the coupling with leads as done in Ref. 13. For example, $\epsilon_1 = E_L - 2|t_c|$, $\epsilon_2 = E_L + U_{LC} - 8t_c^2/(U_0 - U_{LC})$ and $\epsilon_3 = E_L + 2U_{\ell,j} - 3J_{ex}/2 + 2|t_c| + 16t_c^2/(U_0 - U_{LC})$ under the condition $U_0 > U_{LC} \gg t_c$, where $J_{ex} \equiv E_0(S = 3/2) - E_0(S = 1/2)$ is the difference in energy between the spin-3/2 and spin-1/2 configuration.¹³ However, the relative strengths of peaks in the conductance spectrum can only be obtained by solving the full Anderson-Hubbard model self-consistently.

Unlike the G_e spectrum of DQDs,¹⁷ the G_e spectrum of TQDM does not show the electron-hole symmetry due to topological effect. Note that $N = 4$ and $N = 5$ correspond to two-hole and one-hole configurations, respectively. A large Coulomb blockade separation between ϵ_3 and ϵ_4 is given by $\Delta_{34} = U_0 + 3J_{ex} - 4t_c - 8t_c^2/(U_0 - U_{LC})$. Here, ϵ_4 corresponds to the two hole ground state

with spin triplet instead of singlet. The magnitude of G_e is smaller than the quantum conductance $2e^2/h$ for $t_{LR}/\Gamma \gg 1$ as a result of electron Coulomb interactions.¹⁷ The mechanism for understanding the unusual G_e behavior in nanostructure junction systems is a subject of high interest.²⁷ Due to electron Coulomb interactions, the magnitudes of peaks are related to the probability weights of quantum paths, which are related to single-particle occupation numbers and many-particle correlation functions.¹⁸

To reveal the configurations for each main peak, the one-particle occupation number $N_{\ell,\sigma} \equiv \langle n_{\ell,\sigma} \rangle$, inter-dot two particle correlation functions $\langle n_{\ell,\sigma} n_{j,\bar{\sigma}} \rangle$, and three particle correlation functions ($\langle n_{L,\sigma} n_{C,-\sigma} n_{R,\sigma} \rangle$, and $\langle n_{L,\sigma} n_{C,-\sigma} n_{R,-\sigma} \rangle$) are plotted in Fig. 3(b). We always have the relation $N_{L,\sigma} = N_{R,\sigma} \neq N_{C,\sigma}$, because the outer QDs are directly coupled to electrodes, but not the central QD. Such a relation also holds for two-particle and three-particle correlation functions. The six main peaks in Fig. 3(a) indicate the filling of TQDM up to the n -electron ground state for $n = 1, \dots, 6$. For example, ϵ_2 indicates the formation of two-electron state with spin singlet, while ϵ_3 indicates the formation of three-particle state with total spin $S = 1/2$, which can be described as the spin-frustration state^{11,13,28}. Because the on-site Coulomb interaction favors homogeneous distribution of three electrons in TQDM, whereas the interdot Coulomb repulsion favors the charge fluctuation. As seen in Fig. 3(b), for $\Delta_g \leq \epsilon_3$ ($78\Gamma_0$) N_{ℓ} in each dot clearly displays the charge fluctuation behavior. When TQDM goes into a three-particle state ($\Delta_g > \epsilon_3$), the charge fluctuation is suppressed, and each QD is filled with one particle (with $N_{L,\sigma} = N_{R,\sigma} = N_{C,\sigma} = 0.5$), while $\langle n_{L,\sigma} n_{C,\sigma} n_{R,-\sigma} \rangle = \langle n_{L,\sigma} n_{C,-\sigma} n_{R,\sigma} \rangle = \langle n_{L,-\sigma} n_{C,\sigma} n_{R,-\sigma} \rangle$. This also demonstrates the spin frustration condition as depicted in the inset of Fig. 3(a).

Figure 4 shows the charge stability diagram for zero-bias electrical conductance (G_e) and total occupation number (N) as functions of gate voltages exerted on any two QDs (labeled by V_{g1} and V_{g2}) for a TQDM connected to three terminals. The magnitudes of G_e and N are indicated by different colors. It is noticed that G_e is enhanced on the borders that separate domains of different values of occupation number (N) with larger G_e occurring at $V_{g1} = V_{g2}$. This is a result of higher degeneracy and charge-fluctuation in the state. The largest G_e for $N \leq 3$ occurs at the junction between $N = 1$ and $N = 2$ domains when $V_{g1} = V_{g2}$. This feature corresponds to the ϵ_2 peak of Fig. 3(a). The diagram Fig. 4(a) is simply a collection of curves displayed in Fig. 3(a) at different values of V_{g2} that shifts the QD energy levels. We note that in the domains of $N = 1$ and $N = 2$, the areas with stripes

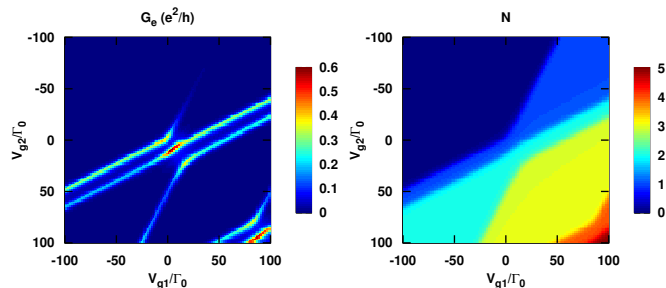


Fig. 4 Charge stability diagram of TQDM. $\Gamma_{\ell} = \Gamma_0$, $k_B T = 1.5\Gamma_0$, $U_{LC} = U_{CR} = U_{LR} = 12\Gamma_0$, $t_{\ell,j} = 3\Gamma_0$. The energy levels are shifted according to $E_{\ell} = E_F - U_{LR} - \sum_{m=1}^2 \beta_{\ell,m} e V_{g_m}$, where the gate coupling constants are $\beta_{L,1} = 0.5$, $\beta_{C,1} = 1$, $\beta_{R,1} = 0.5$, $\beta_{L,2} = 1$, $\beta_{C,2} = 0.5$, and $\beta_{R,2} = 1$.

are not symmetrical with respect to gate voltage. In Ref. 11, a capacitive interaction model was employed to plot the diagram of N . In their model, the electron hopping strength $t_{\ell,j}$ was ignored. Consequently, the charge stability diagram of G_e cannot be obtained. The charge stability diagram of G_e obtained by our full calculation [as shown in Fig. 4(a)] bears close resemblance to the experimental results as shown in Fig. 2 of Ref. 11.

So far, the results shown in Figs. 2-4 are all related to the linear response. To further clarify the QI effect at finite bias ($V_a = 10\Gamma_0$) for different temperatures, we plot in Fig. 5(a) the tunneling current as a function of center QD energy, $E_C = E_F + \Delta_c$ for the configuration shown in the inset of Fig. 5(b). For $\Delta_C \geq 2\Gamma_0$, the tunneling current is suppressed as temperature increases. This is attributed to a reduction of electron population in the electrodes for electrons with energy near $E_F + 10\Gamma_0$. For $\Delta_C \leq 2\Gamma_0$, we notice that $N_{c,\sigma}$ quickly jumps to 0.4, indicating that the central QD is filled with charge, which causes an interdot Coulomb blockade for electrons entering the left QD. (See the reduction of $N_{L,\sigma}$ in Fig. 5(b)). This explains the sharp dip of G_e for $\Delta_C \leq 2\Gamma_0$ in Fig. 5(a). As temperature increases, such a dip in tunneling current is smeared out. At $\Delta_C = 10\Gamma_0 + t_{LC} t_{CR} / t_{LR} \equiv \Delta_{QI}$, the tunneling current vanishes for all temperatures considered due to the QI effect. Such a robust destructive QI effect with respect

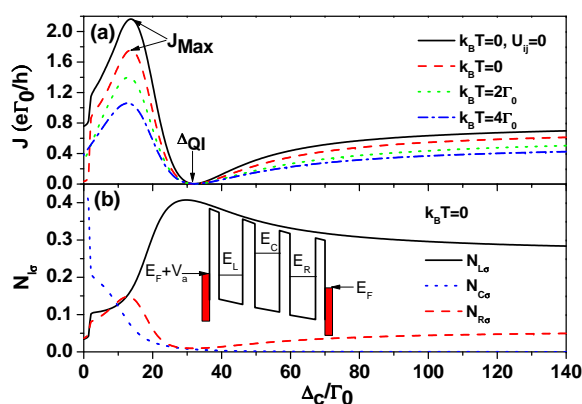


Fig. 5 (a) Tunneling current as a function of $\Delta C = E_C - E_F$ at finite bias $V_a = 10\Gamma_0$ for various temperatures. (b) Occupation numbers as a function of ΔC at $k_B T = 0$. The other physical parameters used are $E_L = E_R = E_F + 10\Gamma_0$, $U_{LC} = U_{CR} = 30\Gamma_0$, $U_{LR} = 10\Gamma_0$, $t_{LC} = t_{CR} = 3\Gamma_0$, $t_{LR} = 0.4\Gamma_0$, and $\Gamma = \Gamma_0$.

to temperature provides a remarkable advantage for the realization of single electron QI transistors at room temperature.¹² To understand the interdot correlation effect, we also plot the case without interdot Coulomb interaction ($U_{\ell,j} = 0$) for $k_B T = 0$ in Fig. 5(a). (See solid curve) We notice that the QI effect remains qualitatively the same, except that the tunneling current is slightly enhanced with interdot Coulomb interaction turned off. As the QI effect suppresses the current flow, the charge will accumulate in the left dot. Thus, $N_{L,\sigma}$ reaches the maximum at $\Delta C = \Delta_{QI}$ while N_R reaches the minimum as seen in Fig. 5(b). This implies that the QI effect can be utilized to control charge storage in TQDM.

4 Conclusions

In summary we have obtained full solution to the charge transport through TQDM junction in the presence of electron Coulomb interactions, which includes all n -electron ($n = 1, \dots, 6$) Green's functions and correlation functions. The destructive and constructive QI behaviors of TQDM are clarified by considering the LDCT effect on the conductance spectrum. The conductance spectrum of TQDM with total occupation number varying from one to six directly reveals the electron-hole asymmetry due to topological effect. The calculated correlation functions also illustrate the charge fluctuation and spin frustration behaviors of TQDM. Our numerical results for charge stability diagram match experimental measure-

ments very well. Finally, we demonstrated that the QI effect in TQDM is robust against temperature variation and it can be utilized to control the charge storage.

Acknowledgments

This work was supported in part by the National Science Council, Taiwan under Contract Nos. NSC 101-2112-M-001-024-MY3 and NSC 103-2112-M-008-009-MY3.

References

- M. A. Reed, C. Zhou, C. J. Muller, T. P. Burgin and J. M. Tour, *Science*, 1997, **278**, 252–254.
- C. Joachim, J. Gimzewski and A. Aviram, *Nature*, 2000, **408**, 541–548.
- J. Bergfield and C. Stafford, *Phys. Rev. B*, 2009, **79**, 245125.
- R. Hanson, L. P. Kouwenhoven, J. R. Petta, S. Tarucha and L. M. K. Vandersypen, *Rev. Mod. Phys.*, 2007, **79**, 1217–1265.
- M. Busl, G. Granger, L. Gaudreau, R. Sánchez, A. Kam, M. Pioro-Ladrière, S. A. Studenikin, P. Zawadzki, Z. R. Wasilewski, A. S. Sachrajda and G. Platero, *Nature nanotechnology*, 2013, **8**, 261–265.
- F. R. Braakman, P. Barthelemy, C. Reichl, W. Wegscheider and L. M. K. Vandersypen, *Nature nanotechnology*, 2013, **8**, 432–437.
- S. Amaha, W. Izumida, T. Hatano, S. Teraoka, S. Tarucha, J. A. Gupta and D. G. Austing, *Phys. Rev. Lett.*, 2013, **110**, 016803.
- A. Nitzan and M. A. Ratner, *Science*, 2003, **300**, 1384–1389.
- C. A. Stafford, D. M. Cardamone and S. Mazumdar, *Nanotechnology*, 2007, **18**, 424014.
- C. Pörtl, C. Emary and T. Brandes, *Phys. Rev. B*, 2013, **87**, 045416.
- M. Seo, H. K. Choi, S.-Y. Lee, N. Kim, Y. Chung, H.-S. Sim, V. Umansky and D. Mahalu, *Phys. Rev. Lett.*, 2013, **110**, 046803.
- C. M. Guédon, H. Valkenier, T. Markussen, K. S. Thygesen, J. C. Hummelen and S. J. van der Molen, *Nature nanotechnology*, 2012, **7**, 304–309.
- M. Korkusinski, I. P. Gimenez, P. Hawrylak, L. Gaudreau, S. A. Studenikin and A. S. Sachrajda, *Phys. Rev. B*, 2007, **75**, 115301.
- C.-Y. Hsieh, Y.-P. Shim and P. Hawrylak, *Phys. Rev. B*, 2012, **85**, 085309.
- Y. Meir and N. S. Wingreen, *Phys. Rev. Lett.*, 1992, **68**, 2512–2515.
- D. M.-T. Kuo and Y.-C. Chang, *Phys. Rev. Lett.*, 2007, **99**, 086803.
- B. R. Bulka and T. Kostyrko, *Phys. Rev. B*, 2004, **70**, 205333.
- D. M.-T. Kuo, S.-Y. Shiao and Y.-C. Chang, *Phys. Rev. B*, 2011, **84**, 245303.
- D. Loss and D. P. DiVincenzo, *Phys. Rev. A*, 1998, **57**, 120–126.
- I. Weymann, B. Bulka and J. Barnaś, *Phys. Rev. B*, 2011, **83**, 195302.
- H. Haug and A.-P. Jauho, *Quantum kinetics in transport and optics of semiconductors*, Springer, 2007.
- D. Goldhaber-Gordon, H. Shtrikman, D. Mahalu, D. Abusch-Magder, U. Meirav and M. A. Kastner, *Nature*, 1998, **391**, 156–159.
- T. Numata, Y. Nisikawa, A. Oguri and A. C. Hewson, *Phys. Rev. B*, 2009, **80**, 155330.

-
- 24 B. Michaelis, C. Emary and C. Beenakker, *EPL (Europhysics Letters)*, 2006, **73**, 677.
- 25 C. Emary, *Phys. Rev. B*, 2007, **76**, 245319.
- 26 D. M. T. Kuo and Y.-C. Chang, *Phys. Rev. B*, 2014, **89**, 115416.
- 27 F. Bauer, J. Heyder, E. Schubert, D. Borowsky, D. Taubert, B. Bruognolo, D. Schuh, W. Wegscheider, J. von Delft and S. Ludwig, *Nature*, 2013, **501**, 73–78.
- 28 S. Andergassen, *Nature*, 2013, **495**, 321–322.